Thermoelectric thiophene dendrimers with large Seebeck coefficients

Journal:	*Molecular Systems Design & Engineering*
Manuscript ID	ME-ART-02-2020-000017.R1
Article Type:	Paper
Date Submitted by the Author:	25-Mar-2020
Complete List of Authors:	Oki, Kota; Kobe University Horike, Shohei; Kobe University, Chemical Science and Engineering Yamaguchi, Mana; Kobe University Takechi, Chikayo; Kobe University Koshiba, Yasuko; Kobe University, Chemical Science and Engineering Fukushima, Tatsuya; Kobe University, Chemical Science and Engineering Mori, Atsunori; Kobe University, Chemical Science and Engineering Ishida, Kenji; Kobe University, Department of Chemical Science and Engineering

MSDE

PAPER

Thermoelectric thiophene dendrimers with large Seebeck coefficients

Received 00th January 20xx,
Accepted 00th January 20xx

DOI: 10.1039/x0xx00000x

Kota Oki,[a] Shohei Horike,*[a,b,c] Mana Yamaguchi,[a] Chikayo Takechi,[a] Yasuko Koshiba,[a] Tatsuya Fukushima,[a] Atsunori Mori,[a,d] and Kenji Ishida*[a,d]

π-conjugated dendrimers are emerging platforms for molecular-based photonics and electronics. Herein, we demonstrate thiophene dendrimers as new thermoelectric (TE) materials with large Seebeck coefficients through chemical charge-carrier doping, conducting film preparation, and TE transport evaluations (electrical conductivity and Seebeck coefficient). Complementary characterization with absorption, photoelectron spectroscopy, and molecular calculations reveal that the highly degenerate frontier molecular orbital energy levels derived from the highly branched and symmetric molecular structures of the dendrimers play an important role in the anomalously large Seebeck coefficient based on Mott's equation. With the recent rapid progress in the technologies for synthesizing π-conjugated dendrimers and molecular designing flexibilities, our results propose a novel strategy for exploring new TE materials.

Design, System, Application

As devices continue to shrink in size and grow in number, the development of power supply methods using clean and abundant elements has become increasingly important. This study investigates a series of dendrimers with thiophene backbones as a new class of thermoelectric (TE) materials. Chemical charge-carrier injection successfully improves the electrical conductivity of the dendrimer films. Owing to the improved electrical conductivity, TE transport of this molecular system could be elucidated for the first time. TE charge-carrier analysis reveals that holes are the major charge-carrier species in p-type doped dendrimers with anomalously large Seebeck coefficient values exceeding that of bismuth alloys. We ascribe the large coefficients to the highly branched and symmetric primary molecular structures, and the characteristic electronic orbitals of the compounds. Our results propose a novel strategy for exploring new TE materials.

Introduction

Dendrimers are repetitively branched macromolecules comprising dendrons that are symmetrically interconnected by a core, forming a spherical morphology.[1–3] Their physicochemical properties, including solubility, reactivity, and crystallinity, can be tuned by adopting functional groups on the molecular surface and/or customizing the core internal functionality. Owing to such molecular design flexibility, these highly branched materials have attracted considerable attention for potential applications in life sciences such as drug delivery, gene delivery, sensors, blood substitution, nanoparticles, crop protection, and agrochemicals.[4–6] In contrast, the potential use of dendrimers in electronics, such as photovoltaics, has received significantly less attention because of their electrically insulating nature.

However, in recent years, a new class of dendrimers bearing a rigid π-conjugated backbone (*e.g.*, phenyl acetylene, phenylene, and thiophene) have been synthesized *via* the Suzuki, Ullmann, or Stille coupling methods, and their unique optical or opt-electrical properties have been investigated.[7–9] For instance, phenyl acetylene and thiophene dendrimers have been characterized by photoluminescence and electroluminescence, and have been demonstrated as energy-funneling media.[7] Phenylazomethine dendrimers complexed with bismuth have shown wavelength-tunable solid-state luminance.[8] In azobenzene-containing aryl ether, the infrared excitation of aromatic units is followed by the channeling of absorbed energy to the core.[9] With such unique functions originating from the branched molecular structures, dendrimers have become more attractive scientific research targets with respect to not only life science but also electronics and photonics.

[a] *Department of Chemical Science and Engineering, Graduate School of Engineering, Kobe University, 1-1 Rokkodai-cho, Nada-ku, Kobe 657-8501, Japan.*
[b] *Nanomaterials Research Institute, National Institute of Advanced Industrial Science and Technology (AIST), 1-1-1 Higashi, Tsukuba 305-8565, Japan.*
[c] *PRESTO, Japan Science and Technology Agency, Kawaguchi 332-0012, Japan.*
[d] *Research Center for Membrane and Film Technology, Kobe University, 1-1 Rokkodai-cho, Nada-ku, Kobe 657-8501, Japan.*

†Electronic Supplementary Information (ESI) available: Used chemicals; synthesis procedures; proton nuclear magnetic resonance data; MALDI-TOF-MS data; four-terminal resistance data; temperature dependence of electrical conductivity; dedoping property; doping level dependence of Seebeck coefficient. See DOI: 10.1039/x0xx00000x

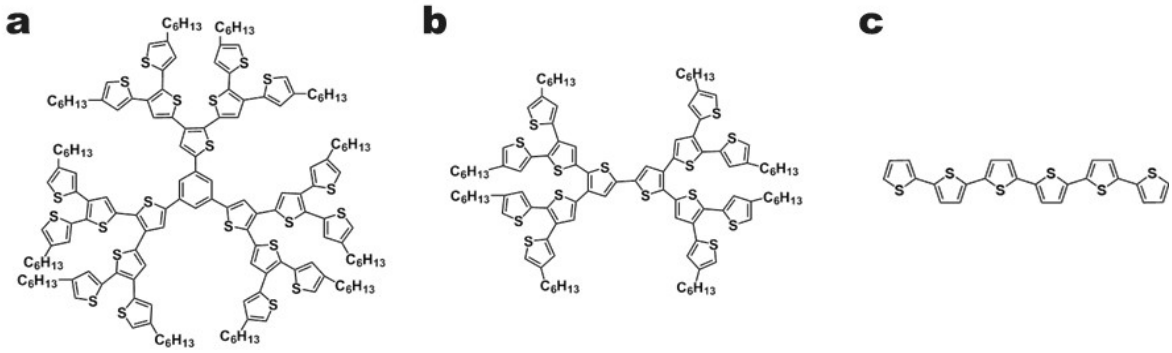

Figure 1. Chemical structures of thiophene derivatives. (a) Ph-(7T)$_3$, (b) 14T, and (c) α-sexithiophene (α-6T). Letter "T" indicates thiophene ring. For instance, three dendrons comprising seven thiophene rings are interconnected by a core benzene ring in Ph-(7T)$_3$. In 14T, the two dendrons are directly homo-coupled. α-6T consists of six linearly connected thiophene rings.

Similar to conducting polymers[10–12], it would be principally possible to give electrical conductivity to dendrimers by charge-carrier injection into their π-conjugated systems *via* chemical, electrochemical, or field-effect doping. This would enable us to study the relationship between their unique and symmetrical molecular structures and carrier transport. One of the technologically useful applications of electrical conductivity is thermoelectric (TE) generation, which converts thermal energy into electric power. The efficiency of TE conversion is evaluated using a dimensionless figure of merit, *ZT*, as follows:[13–15]

$$ZT = \frac{S^2\sigma}{\kappa}T\,. \qquad (1)$$

Here, S is the Seebeck coefficient (output voltage per supplied temperature difference), σ is the electrical conductivity, κ is the thermal conductivity, and T is the temperature. Inorganic semiconducting materials with narrow energy bandgaps, such as bismuth-based alloys, have high *ZT*.[16–18] Thus, these materials are commercially utilized as reserve electric sources and auxiliary power systems. However, they have not been widely used for recent new applications, *e.g.*, energy harvesting, in which energy generators automatically supply electricity for a large number of sensing devices,[19–21] as the lesser element reserves make the compounds highly expensive. It is generally difficult to prepare large-area films of the alloys using low-temperature processes. The brittleness and toxicity also make the components unsuitable for versatile uses and for powering wearable sensors.

Conducting polymers[22–24] and nanoscale-carbon materials[25–27] have recently attracted considerable attention owing to their flexibility, low cost, nontoxicity, light weight, low thermal conductivity, and applicability of wet processes for film preparations. As dendrimers are organic molecules, they provide several of these advantages. Additionally, one of the most interesting points of dendrimers relative to most conducting polymers is their unique electronic structure, which is possibly caused by their highly branched and symmetrical molecular shapes.[7–9] TE transport, particularly the Seebeck coefficient, is quite sensitive to the electronic structures of materials.[28,29] This motivated us to study the TE properties of dendrimers.

Herein, we present the first demonstration of TE behavior by dendrimers with a thiophene backbone, namely, Ph-(7T)$_3$ and 14T (Figure 1a,b). Chemical doping and thin film deposition are carried out using solution-based methods, providing sufficient electrical conductivity for dendrimer films. TE measurements reveal large Seebeck coefficients. An explanation for the large Seebeck coefficient is proposed based on density functional theory (DFT) calculation results. The results predict that the frontier molecular orbital energy levels of the dendrimers are highly degenerate and provide a steep slope of electron density of state (DOS) close to band edges because of their branched and symmetrical structures, unlike a typical linear-shaped thiophene derivative (Figure 1c). With the recent rapid progress in the technologies for synthesizing π-conjugated dendrimers and molecular designing flexibilities, our results propose a novel strategy for exploring new TE materials.

Experimental section

Materials and synthesis of thiophene dendrimers

All materials used for dendrimer synthesis and doping, including the suppliers of the compounds, are summarized in Table S1 of the ESI†. We synthesized Ph-(7T)$_3$ and 14T according to previous reports[30] *via* the Kumada–Tamao–Corriu coupling and homocoupling of 7T dendrons, respectively (see Figures S1, S2, S3, and S4 of the ESI† for details and the proton nuclear magnetic resonance spectra, and matrix-assisted laser desorption/ionization time of flight mass spectrometry data of the products).

Doping and preparation of dendrimer thin films

Ph-(7T)$_3$ and 14T were dissolved in 0.27 mL and 0.11 mL of chloroform, respectively, in 9 mL screw vials (10 mM). Iron (III) chloride hexahydrate ($FeCl_3{\cdot}6H_2O$) was employed as the doping reagent, and it was dispersed in 12 mL of chloroform (0.035 M). Doping was carried out by mixing the dendrimer solution and $FeCl_3{\cdot}6H_2O$ dispersion using a vortex mixer for 10 s. The mixtures were centrifuged at 4,000 rpm for 3 min to remove the residual $FeCl_3$. Cr/Au electrodes with a thickness of 60 nm were vapor-deposited onto quartz glass substrates. The electrodes contained 4-mm gaps for Seebeck measurements, and two-terminal conductivity tests and 110 μm for four-terminal conductivity measurement, respectively. The substrates were 20 mm (length) × 20 mm (width) × 0.5 mm (thickness) in size. Conducting dendrimer thin films were prepared on the substrates by drop casting 90 μL of the solutions while maintaining the substrate surface at 60 °C using a hot plate. The dendrimer films were 6 mm (length) × 6 mm (width) × 0.41–0.72 nm (thickness) in size.

Characterization

The thicknesses of the dendrimer films and Cr/Au electrodes were measured using a step meter (XP-200, Ambios Technology). All

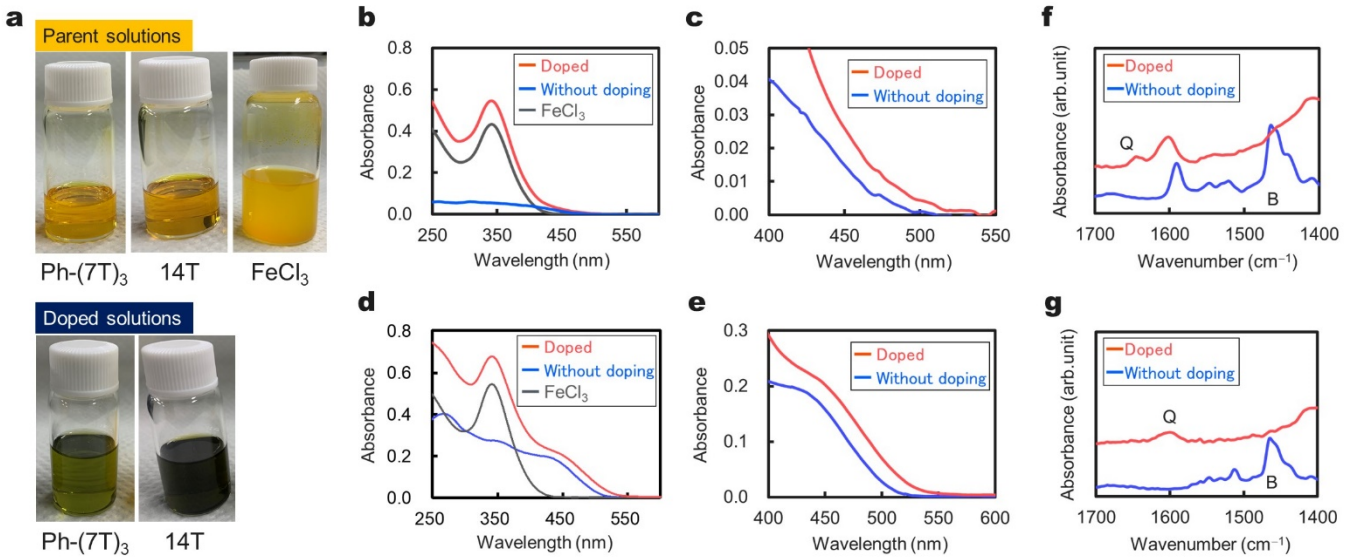

Figure 2. (a) Photographs of chloroform solutions of the dendrimers and $FeCl_3$. Upper and lower panels show the state before and after doping, respectively. UV-vis spectra of (b,c) Ph-$(7T)_3$ and (d,e) 14T. Panels (c) and (e) corresponds to the enlarged views of panels (b) and (d), respectively. FT-IR spectra of (f) Ph-$(7T)_3$ and (g) 14T. Letters "B "and "Q" indicate that these peaks are derived from the benzoid and quinoid structures, respectively.

Seebeck coefficients were measured under vacuum (10^{-2} Pa) by reading the TE voltages from the dendrimer films by utilizing a semiconductor parameter analyzer (B1500A, Keysight Technologies). A specimen was placed on a stage consisting of a ceramic heater and a heat sink. Then, linear temperature gradients were applied in the in-plane directions, with the lower-temperature side maintained constant (300 K). The Seebeck coefficients were obtained from the slopes of TE voltages and temperature differences. The electrical conductivities were measured under DC bias in vacuum (B1500A, Keysight Technologies). The conductivities of the doped and undoped films were measured using four-terminal and two-terminal methods, respectively. The ultraviolet-visible (UV-vis) absorption spectra of the chloroform solutions of the dendrimers were recorded using a quartz cell (V-670, JASCO). The transmission Fourier transform infrared (FT-IR) spectra of the dendrimer films were recorded under vacuum at around 300 K (FT/IR-660 Plus, JASCO). The work functions of the dendrimer films were evaluated using ultraviolet photoelectron yield spectroscopy (UPYS) at approximately 300 K in air (AC-3, Riken Keiki).

Molecular calculation

All molecular calculations were performed based on the DFT using the Gaussian 3.0 package at the B3LYP/6-31G* levels. In our first trial to optimize the molecular structures, the dendrimers seemed to have several local minimums of energy due to a large number of atoms. To reduce computational complexity, hexyl chains were excluded from the calculations, considering that the π-conjugated regions have the most significant contributions to the charge carrier generation and the frontier molecular orbital energies.

Results and discussion

Doping effect and conducting film preparation

First, we studied the doping effect of $FeCl_3$ on the dendrimers. Mixing a conjugated polymer and a doping reagent in solution is a facile doping process. As shown in Figure 2a, the chloroform solutions of the dendrimers exhibit orange-yellow color owing to the π-conjugation of the thiophene moieties.[31] Upon doping with $FeCl_3$ (also yellow-colored dispersion), the color of the solutions immediately transforms into deep blue. These color changes are also observed as the red shifts of the absorption band edges (from 510 to 530 nm for Ph-$(7T)_3$ and from 530 to 560 nm for 14T) in the UV-vis spectra, as shown in Figure 2b–e (red shift). It is well known that the UV-vis absorption peak of π-conjugated polymers and oligomers shifts to a longer wavelength after oxidation or p-doping because of the generation of new electronic states such as polaronic and bipolaronic states.[32,33] Hence, the observed color and spectrum changes apparently indicate charge-carrier injections into the π-conjugated dendrimer systems.

Thiophene-based polymers typically transform from a benzoid to a quinoid structure upon oxidation or p-doping.[34–36] Similar structural changes in thiophene dendrimers could be directly confirmed using FT-IR spectroscopy. The FT-IR spectra (Figure 2f,g) corresponding to the $C_\alpha=C_\beta$ and $C_\beta=C_\beta$ vibrations of thiophene were collected in the neutral and doped states, respectively. The two peaks observed around 1460 and 1510–1520 cm^{-1} (peaks indicated

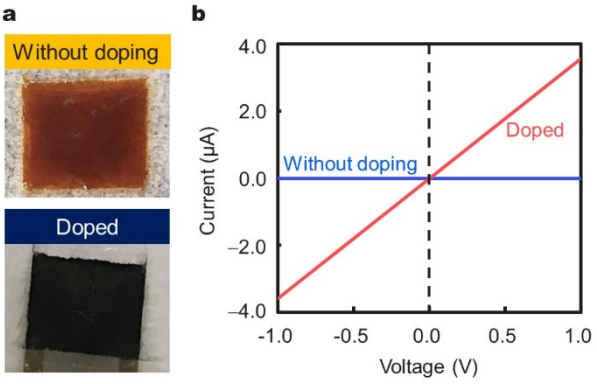

Figure 3. (a) Photographs of 14T films without doping (top panel) and doped with $FeCl_3$ (bottom panel). (b) Representative current–voltage properties of 14T films obtained by the two-terminal method.

as "B" in Figure 2f,g) from the dendrimer films without $FeCl_3$ doping are characteristic of the $C_\alpha = C_\beta$ symmetric and asymmetric stretching vibrations in the neutral thiophene benzoid, respectively. These peaks are not observed for the doped films. Instead, new peaks appear at approximately 1600 cm^{-1} (peaks indicated as "Q" in Figure 2f,g), which are unique to the $C_\beta = C_\beta$ bond. These new peaks suggest the generation of the quinoid structure by $FeCl_3$ doping. Note that the peak at approximately 1590 cm^{-1} observed from the Ph-$(7T)_3$ film without doping would be assigned as the ring stretch vibration of the core benzene,[37] which still can be seen after $FeCl_3$ doping.

As shown in Figure 3a, the doped dendrimer films exhibit a deep blue color while the pristine films are orange-yellow in color; the doped states are maintained after the film preparation. Representative resistance measurement results by the two-terminal method are shown in Figure 3b. It can be seen that the doped films are more conductive than the undoped films, showing at least an 8.5 million-fold increase in electric current under the same applied biases. The four-terminal conductivities of doped Ph-$(7T)_3$ and 14T are 2.38×10^{-5} and 7.43×10^{-4} S cm^{-1}, respectively (see Figure S5 of the ESI† for the actual voltage drop–applied current properties). The charge-carrier generations are responsible for this improvement in conductivity. Moreover, the temperature dependence of the electrical conductivities of the dendrimer films showed typical Arrhenius-type behavior (Figure S6, ESI†), suggesting hopping conduction in the dendrimer films. Unfortunately, the obtained conductive thiophene dendrimers easily suffered from dedoping (for detail, see Figure S7, ESI†); however, to the best of our knowledge, this is the first attempt at exploring the effect of doping on π-conjugated dendrimers and preparing their conducting films.

TE properties and transport in doped thiophene dendrimers

We could measure the Seebeck coefficients of the dendrimer films because of the improvement in electrical conductivities caused by doping. The voltage output from the doped dendrimer films is proportional to the supplied temperature difference, as shown in Figure 4a. The positive sign of the coefficient indicates that holes are the major charge-carrier species for Ph-$(7T)_3$ and 14T. This corresponds to the p-doping by $FeCl_3$ and the moving of Fermi levels close to the valence bands. The obtained coefficients are 343 μV K^{-1} for Ph-$(7T)_3$ and 135 μV K^{-1} for 14T; 343 μV K^{-1} is one of the largest values obtained among the organic compounds[38,39] tested until now, and it exceeds the value for bismuth alloys.[40,41] The obtained Seebeck coefficients were decreased by addition of $FeCl_3$, thereby increasing the number of holes. The power factor, $P = S^2\sigma$, is 2.8×10^{-4} and 1.3×10^{-3} μW m^{-1} K^{-2} for Ph-$(7T)_3$ and 14T, respectively. These values are approximately two to five orders of magnitude lower compared to the commercially available inorganic materials and recent conducting polymers (*e.g.*, poly(3,4-ethylenedioxythiophene)) because of the lower electrical conductivities of the dendrimers. However, this study emphasizes that the Seebeck coefficient can be significantly improved through primary molecular structure designing.

It should be noted the Seebeck coefficient increases with the branching and symmetry of molecular structures, as shown in Figure 4b (Ph-$(7T)_3$ > 14T > α-6T[42]), even though the constituent π-conjugated backbone is the same thiophene. Therefore, the present large Seebeck coefficients observed in the dendrimers could be explained by their characteristic electronic structures resulting from their branched and symmetric molecular structures. To verify this consideration, we created the energy diagram of the dendrimers and α-6T in undoped states through DFT calculations, as shown in Figure 4c. We focused on the highest occupied molecular orbital (HOMO) and the lowest unoccupied molecular orbital (LUMO) energy levels. The number of orbitals existing close to the band edges, *i.e.*, degeneracy, increases with the symmetry of the molecular structures. Particularly for Ph-$(7T)_3$, which has 3-fold rotational symmetry, the HOMO and LUMO energy levels are triply degenerate. This enhanced degeneracy is suitable because an electron has the same energy levels in a symmetric space. The HOMO mapping shown in Figure 4d also supports the degeneracy in Ph-$(7T)_3$, in which the HOMO, HOMO−1, HOMO−2 clouds unevenly distribute on three dendrons. The HOMO of 14T and α-6T do not show such biased

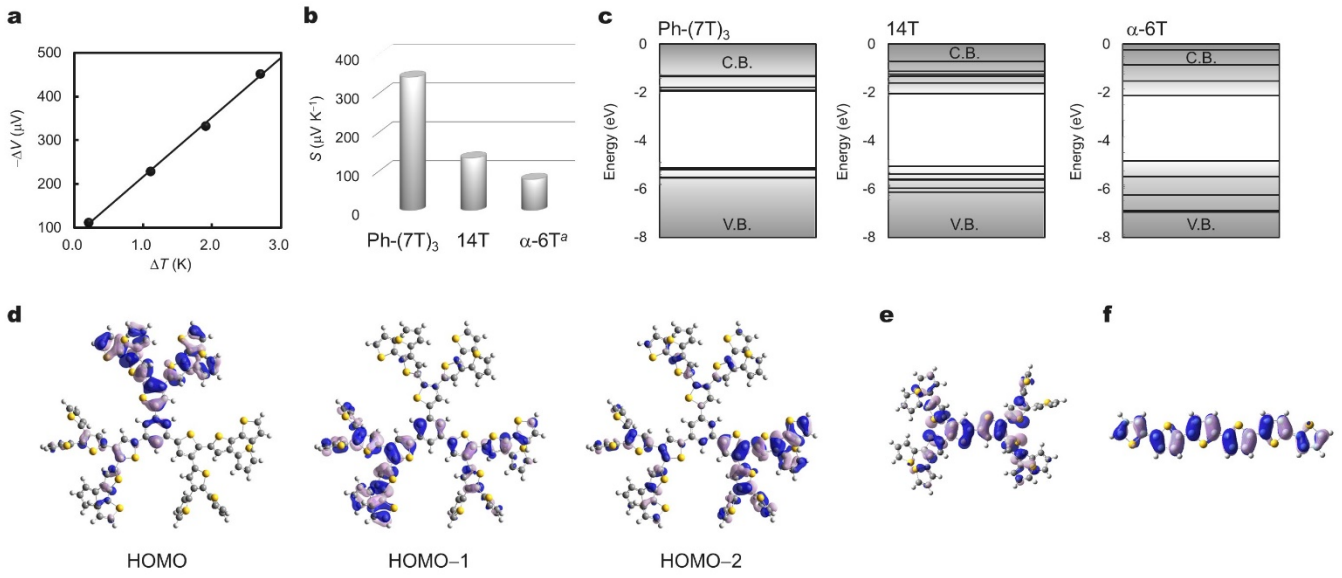

Figure 4. (a) Representative ΔV-ΔT plot of doped 14T film. (b) Comparison of Seebeck coefficients of Ph-$(7T)_3$ and 14T doped with $FeCl_3$, and α-6T. [a]From Tagani.[39] (c) Energy diagrams of Ph-$(7T)_3$, 14T, and α-6T. V.B. and C.B. indicate valence band and conduction band, respectively. HOMO mappings of (d) Ph-$(7T)_3$, (e) 14T, and (f) α-6T obtained by DFT calculations. Gray, white, and yellow color balls indicate carbon, hydrogen, and sulfur atoms, respectively. Light purple and blue colors indicate positive and negative phases of the orbitals, respectively.

distribution (Figure 4e,f); and therefore, the relatively enhanced degeneracy of 14T compared to α-6T is attributed to the branched structures and the increased number of atoms.

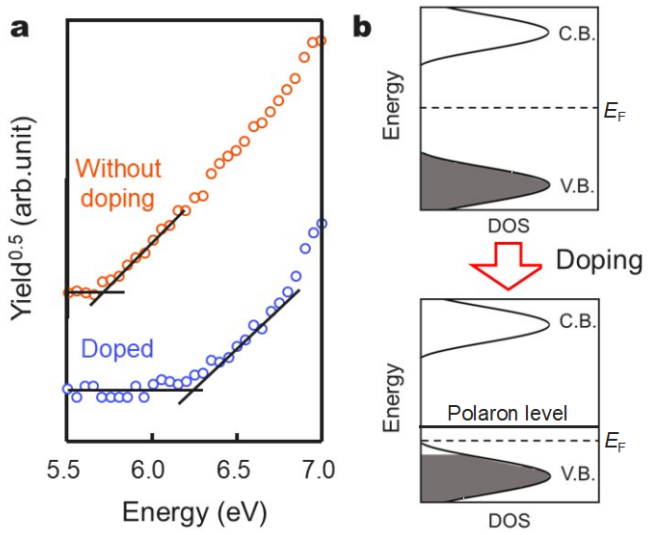

Figure 5. (a) UPYS spectra of Ph-(7T)$_3$ films recorded for the doped and undoped states. (b) Schematic of Fermi energy level shift toward the valence band edge in dendrimers upon hole doping.

The enhanced degeneracy contributes to the increase in the DOS of electrons. TE transport is mathematically expressed by Mott's equation,[43,44] in which the Seebeck coefficients directly reflect the DOS shape at the Fermi level as:

$$S \propto -\frac{\pi^2}{3}\frac{k_B^2 T}{q}\left[\frac{\partial \ln[N(E)]}{\partial E}\right]_{E=E_F}, \quad (2)$$

where E is the energy, E_F is the energy of the Fermi level, k_B is the Boltzmann constant, q is the elementary charge, and $N(E)$ is the DOS at energy E. Mott's equation suggests that a large Seebeck coefficient is achieved by a local increase in the DOS, which leads to a large $\partial \ln[N(E)]/\partial E$. In the case of semiconductors, the Seebeck coefficient is expected to be maximized when a Fermi level moves close to a band edge.[43,44]

In the present study, the Fermi levels of the dendrimers should move close to the HOMO because of the hole doping (electron withdrawing) by $FeCl_3$. UPYS spectra were measured to elucidate this energy level shift in the thiophene dendrimers, as shown in Figure 5a. The onset energy in the spectra, corresponding to the HOMO energy level, is −5.73 for Ph-(7T)$_3$ without doping. This value is slightly different from those obtained by DFT calculations (Figure 4c); however, high-energy shifts (0.50 eV) can be seen in the doped dendrimer film. This result demonstrates the p-type doping and accompanied Fermi level shifts toward the valence band edges of the dendrimers, as schematically illustrated in Figure 5b. The Seebeck coefficient is effectively improved through Mott's equation. The order of the Seebeck coefficient in the present thiophene derivatives (Ph-(7T)$_3$ > 14T > α-6T[42]) can be explained by the difference in degeneracy of the HOMO energy levels. Finally, it is worth noting that electrical conductivity is generally proportional to charge-carrier density, while the Seebeck coefficient decreases with the increase in charge-carrier density. Therefore, the present results, in which conductivity and the Seebeck coefficient are simultaneously enhanced by doping, are considered as a rare case.

Conclusions

We present the first experimental demonstration of the charge-carrier doping of thiophene dendrimers and their TE behaviors. Large positive Seebeck coefficients are obtained at 300 K, suggesting hole injection and transport in the dendrimer thin films. These large coefficients are explained by the steep DOS slopes that originate from the symmetric molecular textures using DFT calculations. Our results demonstrate π-conjugated dendrimers as a new class of TE materials, emphasizing the potential capability for molecular design to be used as an efficient toolbox for exploring and developing future TE materials.

Conflicts of interest

There are no conflicts to declare.

Acknowledgements

This work was supported in part by JSPS KAKENHI (No. 17J00903 and No. 19H02608). UPYS measurement was performed in NAIST, supported by the Nanotechnology Platform Program (Synthesis of Molecules and Materials) of the Ministry of Education, Culture, Sports, Science, and Technology (MEXT), Japan.

References

1 D. A. Tomalia, H. Baker, J. Dewald, M. Hall, G. Kallos, S. Martin, J. Roeck, J. Ryder and P. Smith, *Polym. J.*, 1985, **17**, 117.
2 B. Klajnert and M. Bryszewska, *Acta Biochim. Pol.*, 2001, **48**, 199.
3 D. A. Tomalia and J. M. J. Fréchet, *J. Polym. Sci. Pol. Chem.*, 2002, **40**, 2719.
4 E. R. Gillies and J. M. J. Fréchet, *Drug Discov. Today*, 2005, **10**, 35.
5 R. Duncan and L. Izzo, Adv. *Drug Deliver. Rev.*, 2005, **57**, 2215.
6 H.-L. Fu, S.-X. Cheng, X.-Z. Zhang and R.-X. Zhuo, *J. Gene Med.*, 2008, **10**, 1334.
7 M. I. Ranasinghe, M. W. Hager, C. B. Gorman and T. Goodson, *J. Phys. Chem. B*, 2004, **108**, 8543.
8 T. Kambe, A. Watanabe, T, Imaoka and K. Yamamoto, *Angew. Chem. Int. Edit.*, 2016, **55**, 13151.
9 D.-L. Jiang and T. Aida, *Nature*, 1997, **388**, 454.
10 C.-J. Yao, H.-L. Zhang, and Q. Zhang, *Polymers,* 2019, **11**, 107.
11 J. Ding, Z. Liu, W. Jin, L. Xiang, Z. Wang, Y. Zeng, Y. Zou, F. Zhang, Y. Yi, Y. Diao, C. R. McNeill, C.-A. Di, D. Zhang, and D. Zhu, *Angew. Chem.,* 2019, **131**, 19170.
12 Q. Zhang, Y. W. Xu, and D. Zhu, *Adv. Mater.,* 2014, **26**, 6829.
13 H. J. Goldsmid, Thermoelectric Refrigeration, Plenum, New York, 1964.
14 D. M. Rowe, CRC Handbook of Thermoelectrics, CRC Press, Boca Raton, 1995.
15 A. F. Ioffe, Physics of Semiconductors, Academic Press, New York, 1960.
16 D.-Y. Chung, T. Hogan, P. Brazis, M. Rocci-Lane, C. Kannewurf, M. Bastea, C. Uher and M. G. Kanatzidis, *Science*, 2000, **287**, 1024.
17 R. Venkatasubramanian, E. Siivola, T. Colpitts and B. O'Quinn, *Nature*, 2001, **413**, 597.
18 B. Poudel, Q. Hao, Y. Ma, Y. Lan, A. Minnich, B. Yu, X. Yan, D. Wang, A. Muto, D. Vashaee, X. Chen, J. Liu, M. S. Dresselhaus, G. Chen and Z. Ren, *Science*, 2008, **320**, 634.

19 O. Bubnova and X. Crispin, *Enrg. Environ. Sci.,* 2012, **5**, 9345.
20 N. E. Dutoit, B. L. Wardle and S.-G. Kim, *Integr. Ferroelectr.* 2006, **71**, 121.
21 J. Li, H. Yu, S. M. Wong, G. Zhang, X. Sun, P. G.-Q. Lo and D.-L. Kwong, *Appl. Phys. Lett.,* 2009, **95**, 033102.
22 G. A. Snook, P. Kao and A. S. Best, *J. Power Sources*, 2011, **196**, 1.
23 J. Stejskal and R. G. Gilbert, *Pure Appl. Chem.*, 2009, **74**, 857.
24 J. Roncali, *Chem. Rev.*, 1992, **92**, 711.
25 R. H. Baughman, A. A. Zakhidov and W. A. de Heer, *Science*, 2002, **297**, 787.
26 A. H. C. Neto, F. Guinea, N. M. R. Peres, K. S. Novoselov and A. K. Geim, *Rev. Mod. Phys.*, 2009, **81**, 109.
27 S. Horike, T. Fukushima, T. Saito, T. Kuchimura, Y. Koshiba, M. Morimoto and K. Ishida, *Mol. Syst. Des. Eng.*, 2017, **2**, 616.
28 J. P. Heremans, V. Jovovic, E. S. Toberer, A. Saramat, K. Kurosaki, A. Charoenphakdee, S. Yamanaka and G. J. Snyder, *Science*, 2008, **321**, 554.
29 T. Takeuchi, T. Kondo, T. Takami, H. Takahashi, H. Ikuta, U. Mizutani, K. Soda, R. Funahashi, M. Shikano, M. Mikami, S. Tsuda, T. Yokoya, S. Shin and T.Muro, *Phys. Rev. B*, 2004, **69**, 125410.
30 S. Tanaka, D, Tanaka, G. Tatsuta, K. Murakami, S. Tamba, A. Sugie and A. Mori, *Chem. Eur. J.*, 2013, **19**, 1658.
31 C. Xia, X. Fan, J. Locllin, R. C. Advincura, A. Gies and W. Nonidez, *J. Am. Chem. Soc.,* 2004, **126**, 8735.
32 R. Kroon, D. Kiefer, D. Stegerer, L. Yu, M. Sommer and C. Müller, *Adv. Mater.*, 2017, **29**, 1700930.
33 D. T. Scholes, S. A. Hawks, P. Y. Yee, H. Wu, J. R. Lindemuth, S. H. Tolbert and B. J. Schwartz, *J. Phys. Chem. Lett.*, 2015, **6**, 4786.
34 C. X. Cui and M. Kertesz, *Phys. Rev. B*, 1989, **40**, 9661.
35 J. Casado and J. T. L. Navarrete, *Chem. Rec.*, 2011, **11**, 45.
36 G. Zotti, S. Zecchin, B. Vercelli, A. Berlin, J. Casado, V. Hernández, R. P. Ortiz, J. T. L. Navarrete, E. Ortí, P. M. Viruela and B. Milián, *Chem. Mater.*, 2006, **18**, 1539.
37 D. Syomin, J. Kim, B. E. Koel and G. B. Ellison, *J. Phys. Chem. B,* 2001, **105**, 8387.
38 Y. Nakai, K. Honda, K. Yanagi, H. Kataura, T. Kato, T. Yamamoto and Y. Maniwa, *Appl. Phys. Express*, 2014, **7**, 025103.
39 G.-H. Kim, L. Shao, K. Zhang and K. P. Pipe, *Nat. Mater.*, 2013, **12**, 719.
40 D. Kusano and Y. Hori, *J. Japan Inst. Metals*, 2002, **66**, 1063.
41 G. E. Smith and R. Wolfe, *Jpn. J. Appl. Phys.*, 1962, **33**, 841.
42 M. B. Tagani, *J. Phys. D Appl. Phys.*, 2016, **49**, 125302.
43 A. D. Avery, B. H. Zhou, J. Lee, E.-S. Lee, E. M. Miller, R. Ihly, D. Wesenberg, K. S. Mistry, S. L. Guillot, B. L. Zink, Y.-H. Kim, J. L. Blackburn and A. J. Ferguson, *Nat. Energy*, 2016, **1**, 16033.
44 M. Nakano, T. Nakashima, T. Kawai and Y. Nonoguchi, *Small*, 2017, **13**, 1700804.